Optimization of a Microscale, Axial-Flux, Permanent-Magnet Generator

D. P. Arnold[1*], I. Zana[1†], F. Herrault[1], P. Galle[1], J.-W. Park[1], S. Das[2], J. H. Lang[2], and M. G. Allen[1]
[1]School of Electrical and Computer Engineering, Georgia Institute of Technology, Atlanta, GA 30332, USA
Phone: (404) 894-9419, Fax: (404) 894-5028, Email: mark.allen@ece.gatech.edu
[2]Dept. of Electrical Eng. and Computer Science, Massachusetts Institute of Technology, Cambridge, MA, 01239, USA
[*]now with Dept. of Electrical and Computer Engineering, University of Florida, Gainesville, FL, 32611, USA
[†]now with Center for Materials for Information Technology, University of Alabama, Tuscaloosa, AL, 35487, USA

Abstract

This paper presents the design optimization and characterization of a microscale, permanent-magnet (PM) generator, capable of supplying 8 W of DC power to a resistive load at a rotational speed of 305,000 rpm. The generator is a three-phase, axial-flux, PM machine, consisting of a stator with Cu surface windings and a multi-pole SmCo PM rotor. Optimization of the machine geometries have resulted in a 30% improvement in power density over a previously reported machine (at 120,000 rpm). Furthermore, these design improvements in combination with higher rotational speeds has enabled a >7x improvement in total output power and a net power density of 59 W/cm^3.

Keywords: power generator, magnetic generator, permanent-magnet machine, FEMLAB finite element modeling

1. INTRODUCTION

Microscale, axial-flux, PM generators are an active area of research for high power density electromechanical energy conversion. These devices are of particular interest because their planar geometry merges well with MEMS fabrication techniques. These electrical power converters require input mechanical power, and hence rely on power from an integrated turbine or some other mechanical power source, such as a gas-fueled turbine engine [1].

We have previously reported a first-generation microscale, axial-flux, PM generator that demonstrated 2.6 W of mechanical-to-electrical power conversion and delivery of 1.1 W of DC power to a resistive load at a rotor speed of 120 krpm using a 9.5 mm diameter SmCo rotor [2]. We have also reported methods to increase the rotational speeds and thus boost the output power by improving the rotor mechanical integrity [3]. Other groups have also investigated micromachined planar PM generators. One has demonstrated a self-contained flow-driven generator that produced 1.1 mW at 30 krpm for a 7.5 mm diameter rotor containing small NdFeB magnets [4]. Another has reported 14.6 mW output power for an 8 mm diameter machine at 58 krpm using a NdFeB rotor [5], but in the corresponding conference presentation, presented late-breaking results of 5 W of power at 380 krpm.

Rare-earth PMs (e.g. SmCo, NdFeB) are the rotor material of choice for these devices because the high energy products offer the highest electromechanical power conversion. However, when considering future integration of the generator in a high-temperature microengine [1], SmCo is preferred (over NdFeB) for its high Curie temperature and low remanence loss at elevated temperatures.

Thus, in furtherance of these efforts, we now report a redesigned, second-generation generator having a similar construction, but with optimized machine geometries. This paper highlights the design considerations and fabrication tradeoffs required to maximize the output power through optimization of the overall machine geometry and stator winding patterns.

2. MACHINE OVERVIEW

The generator is a three-phase, eight-pole, axial-flux, synchronous machine comprised of a rotor with an annular PM and soft magnetic back iron and a stator with Cu surface windings on a magnetically soft substrate, which serves as a magnetic back iron.

The stator uses interleaved, electroplated Cu windings that are dielectrically isolated from a 1-mm thick NiFeMo substrate by a 5-µm polyimide layer (Fig.1). The rotor contains an eight-pole, 500 µm thick, annular SmCo PM and a 500 µm thick FeCoV (Hiperco 50) back iron. For this design, both the rotor magnet and back iron have an inner diameter of 5 mm, and an outer diameter of 10 mm.

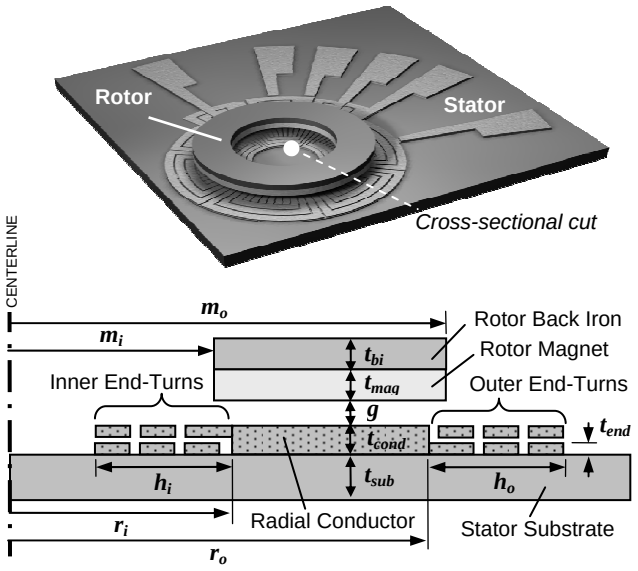

Figure 1. Axial-flux permanent-magnet machine perspective and cross-sectional schematics.

3. DESIGN IMPROVEMENTS

There are several design improvements in the second-generation device aimed at reducing the winding resistances by making more effective use of the available volume (between the rotor magnet and stator substrate). First, the radial conductor segments occupy the full thickness of both metal layers, as depicted in Figs. 1 and 2. They are thicker, 200 μm rather than ~100 μm, and therefore have lower resistance. Second, the inter-conductor spacing was reduced from 130 μm to 50 μm, further increasing the Cu cross-sectional area for lower resistance. Third, the radial conductors were shortened by 500 μm relative to the rotor magnet radial span, permitting optimal flux linkage of radial leakage flux while minimizing the total coil length.

The new design also features a more effective winding pattern with an improved end-turn connection scheme, as shown in Fig. 3. The number of "crossovers" and thus vias was reduced (from 96 to 3) by using variable-pitch coils and permitting each end turn segment to occupy only one layer (either top or bottom). Also, each end-turn segment width, length, and shape were optimized for minimum overall resistance.

4. MACHINE OPTIMIZATION

The design goal is to maximize the flux linkage between the rotor and stator for maximum induced voltage while minimizing the stator winding resistance for maximum output power. For a generator of a fixed volume operating at a constant rotational speed, first-order analysis indicates that output power scales independently of the number of poles (p) and number of winding turns/pole (n)—increasing either has the effect of increasing the output voltage while simultaneously increasing the winding resistance. However, when design and fabrication limitations are introduced, the simple first-order approximations do not hold.

Therefore a parametric optimization was performed to find the optimum values for p and n along with the corresponding optimal winding pattern geometries for maximum output power. Both p and n were varied while enforcing certain microfabrication constraints for the rotor and stator (Table 1). The radial dimensions of the magnet were fixed, as were all axial parameters (e.g. air gap, thicknesses, etc.). A four-step procedure was used.

1. For each combination of p and n, the inner and outer end-turn extensions, h_i and h_o, were varied to find the winding pattern that yielded the lowest electrical resistance. The relative resistance contribution of each winding segment (radial conductors, inner end turns, and outer end turns) as well as the total resistance was also calculated using geometrical relations using a resistivity of $\rho_{Cu} = 1.7$ μΩ·cm.

2. For each value of p, a 3-D, nonlinear, finite-element model (FEM) was used (FEMLAB) to solve for the static magnetic B-fields in the machine. The rotor was modeled using an ideal magnetization with a remanence of $B_r = \pm 1$ T and relative permeability of $\mu_r = 1$. The FeCoV back iron

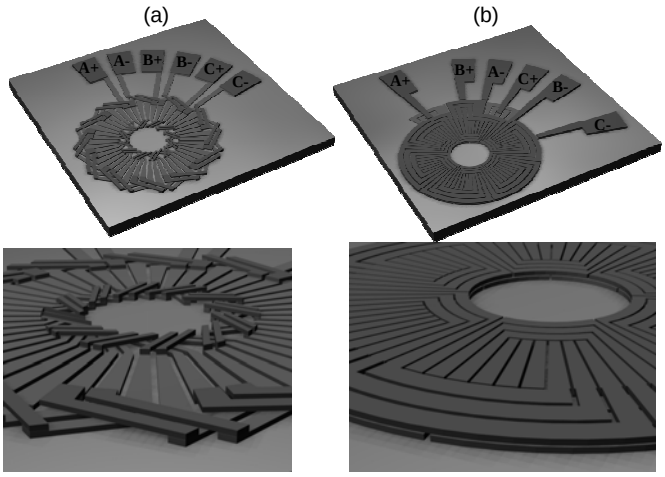

Figure 2. Stator winding patterns for (a) original, 8-pole, 2-turn/pole and (b) optimized, 8-pole, 3-turn/pole.

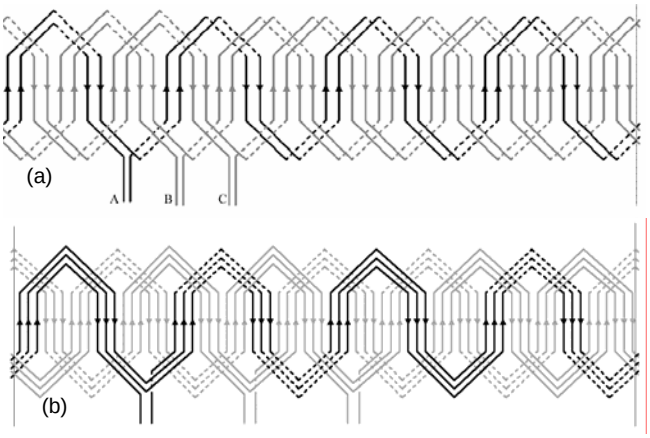

Figure 3. A comparison of the winding diagrams for the (a) 2-turn/pole original machine and (b) 3-turn/pole optimized machine. Solid lines represent layer 1 and dashed lines, layer 2. Phase A is darkened for reference.

Table 1. Optimization parameters.

FIXED PARAMETERS			
Parameter	***Description***	***Value***	***Units***
m_o	Magnet outer radius	5.0	mm
m_i	Magnet inner radius	2.5	mm
r_o	Stator radial conductor outer radius	4.75	mm
r_i	Stator radial conductor inner radius	2.75	mm
t_{bi}	Back iron thickness	500	μm
t_{mag}	Magnet thickness	500	μm
t_{cond}	Radial conductor thickness	200	μm
t_{end}	End turn thickness	80	μm
t_{sub}	Substrate thickness	1000	μm
g	Air-gap	100	μm
w_{min}	Minimum feature width	50	μm
R_{pe}	Power electronics equiv. resistance	100	mΩ

VARIABLE PARAMETERS			
Parameter	***Description***	***Range***	***Units***
p	# poles	2 - 12	-
n	# turns/pole	1 - 6	-
h_o	Outer end-turn extension	0 - 2.5	mm
h_i	Inner end-turn extension	0 - 2.5	mm

and NiFeMo stator substrate were modeled using experimentally measured nonlinear material properties. The model employed two magnetic half-poles and enforced periodic boundary conditions, as shown in Fig. 4.

3. Using the optimized winding dimensions and the results from the FEM, the induced voltage waveforms and rms voltages were computed. This was accomplished using a MATLAB script to numerically integrate the B-field to find the flux through an area defined by the shape of the coil. The integration area was then "rotated" in 1° step increments to simulate the relative motion of the rotor. This process was used to determine time rate of change of flux through the coil, and hence the induced single-phase open-circuit voltage.

4. The rms value of the open-circuit voltage was then applied to a matched-load circuit model using a series equivalent resistance of 100 mΩ to account for losses in the power electronics.

Fig. 5 shows the matched-load output power, normalized by the maximum, indicating that 8-pole, 3 turn/pole is the optimal configuration. The unplotted regions indicate geometries that exceed the limitations of the fabrication design rules, i.e. the conductors are too narrow.

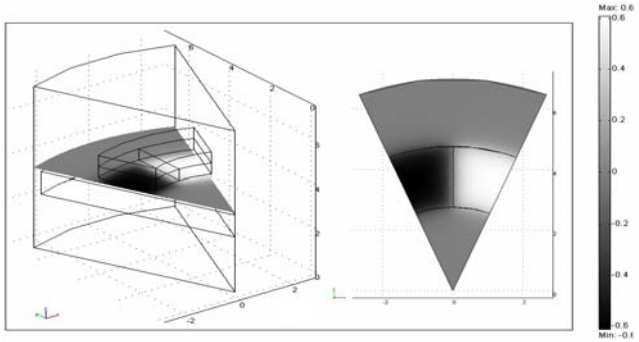

Figure 4. FEMLAB finite element model results showing the z-directed B field 100 µm above the stator surface for the case of p=8.

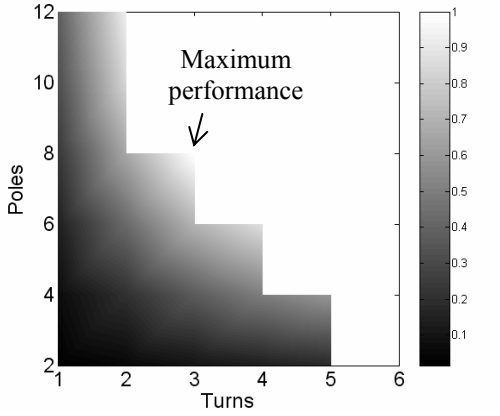

Figure 5. Matched-load three-phase output power, normalized by the maximum, at 305 krpm, indicating maximum performance for 8-pole, 3-turn/pole stator.

5. FABRICATION

To confirm an improvement in the overall design, optimized stators were built using previously reported [2] methods. The final device consisted of two electroplated Cu layers, 80 µm and 60 µm thick, respectively, insulated by 40 µm of SU8, as shown in Fig. 6. The fabricated geometry differs from the modeled geometry (80 µm Cu layers with 20 µm insulation) due to process variations. The single-phase winding resistance and inductance for this optimized machine are 160mΩ and 0.31 µH, respectively, higher than the projected values of 100 mΩ and 0.138 µH.

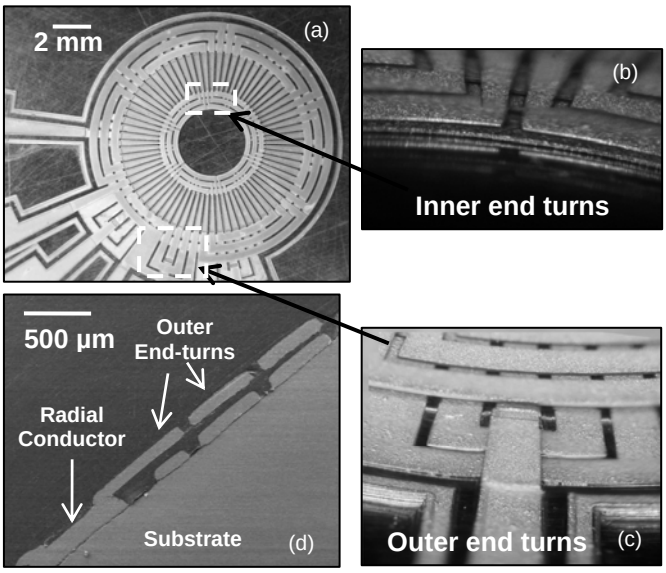

Figure 6. (a) Fabricated 3-turn, 8-pole stator, (b) Close-up on inner end-turns, (c) Close-up of outer end-turns and electrical connection arm, (d) SEM cross-section of machines (compare with Figure 1).

6. RESULTS

Using the test stand and approaches described in [2], electrical characterizations were performed. The open-circuit voltage V_{oc} is linear with speed and decays with air gap, as depicted in Fig. 7. The experimental values are seen to closely match analytical models.

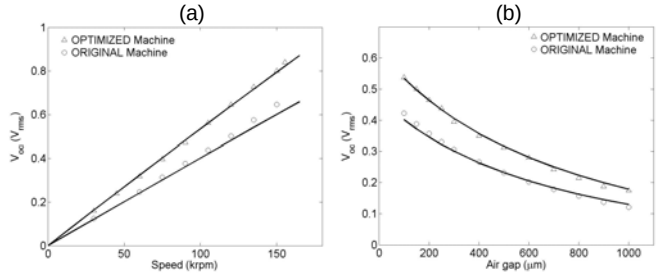

Figure 7. Open-circuit voltages (a) vs rotational speed for 100 µm air gap and (b) vs. air gap at 100,000 rpm for original and optimized machines. Data points represent measurements; lines represent analytical model.

The new, optimized machine exhibits a 26% higher open-circuit voltage as compared to the original machine. This increase ideally should be 50% (3 turns/pole rather than 2 turns/pole), assuming equal magnetic properties, magnetic surface area, and magnetic gap. However, the original machine possessed a 9% larger magnet surface area (3.2 mm ID, 9.5 mm OD, compared to 5 mm ID, 10 mm OD). In addition, the magnets were manufactured by two different vendors, and may not possess equal magnetic properties. Also, there is some variation in the magnetic gap. Therefore, a direct comparison of performance is difficult.

For power measurements, the air gap was fixed at 100 μm. A passive AC/DC converter, comprising a three-phase Δ/wye-connected (1:6 turns ratio) transformer and a three-phase diode bridge rectifier, was used to provide DC power to a resistive load [2]. The output power was measured as a function of load resistance at 100 krpm to find the peak output power (matched-load condition). The load was then fixed, and the power was measured as a function of speed. The load resistance was re-measured at each speed to ensure accuracy as the resistor heated.

For these experiments, a maximum DC output power of 8 W was achieved at 305 krpm for a matched 37 Ω load, as shown in Fig. 8. For an active volume of 136 mm^3 (OD=10 mm, ID=5 mm, thickness=2.3 mm), this corresponds to a power density of 59 W/cm^3.

The predicted electrical, η_e, and generator, η_g, system efficiencies [2] under maximum power transfer conditions (i.e. matched-load) are shown in Fig. 9 as a function of speed. The electrical system efficiency, which neglects magnetic eddy current losses in the substrate, approaches the ideal 50% as the speed increases. This shows how transformer core losses and diode voltage drop losses in the AC/DC converter become less significant with increasing speed. The generator system efficiency is smaller than the electrical system efficiency due to eddy current losses in the stator core. This indicates the need for magnetic laminations in the stator.

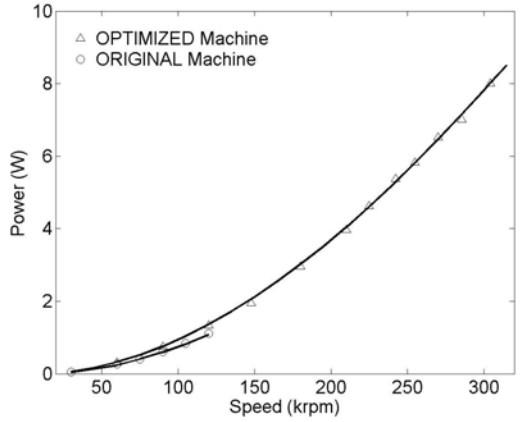

Figure 8. Matched-load DC output power for original and optimized machines. Data points represent measurements; lines represent analytical model.

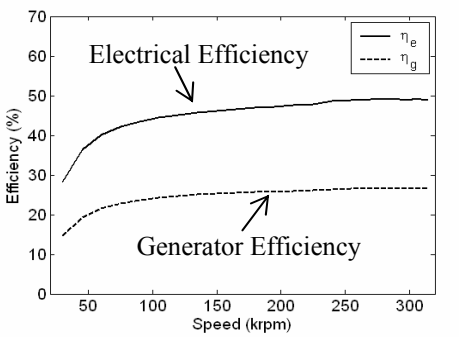

Figure 9. Electrical system efficiency, η_e, and generator system efficiency, η_g, vs. speed (matched-load conditions).

7. CONCLUSIONS

The optimized machine demonstrated 16 W of mechanical-to-electrical power conversion and delivery of 8 W of DC power to a resistive load at a rotational speed of 305 krpm (59 W/cm^3 power density). A maximum power of 1.1 W was achieved for the first-generation machine at 120 krpm [2]. At the same speed, the second-generation machine demonstrates 1.3 W and a corresponding 30% improvement in power density attributed solely to stator enhancements. Combining these stator improvements with the higher rotational speeds (305 krpm) enabled a 7.2x improvement in total output power. These speeds represent improvement compared to the highest speeds previously reported [2,3], but unfortunately, at 305 krpm, the SmCo permanent magnet suffered catastrophic mechanical failure and destroyed the stator.

Future work will continue to focus on improving the power electronics, reducing substrate eddy current losses, and determining the machine performance at elevated temperatures. Other work may focus on investigating NdFeB rotors for potential low-temperature applications.

ACKNOWLEDGMENTS

This work was supported by the United States Army Research Laboratory Collaborative Technology Alliance (DAAD19-01-2-0010).

REFERENCES

[1] S. A. Jacobson and A. H. Epstein, "An informal survey of power MEMS," *ISMME 2003*.

[2] S. Das, et al., "Multi-watt electric power from a microfabricated permanent-magnet generator," *IEEE MEMS 2005*, pp. 287-290.

[3] D. Arnold, et al., "High-speed characterization and mechanical modeling of microscale, axial-flux, permanent-magnet generators," *Transducers '05*, pp. 701-704.

[4] A. S. Holmes, et al., "Axial-flux permanent magnet machines for micropower generation," *J. Microelectromech. Syst.*, vol. 14, no. 1, pp. 54-62, Feb. 2005.

[5] H. Raisigel, et al., "Magnetic planar micro generator," *Transducers '05*, pp. 757-761.